CROSS-WIRE CALIBRATION FOR FREEHAND 3D ULTRASONOGRAPHY

A. Anagnostoudis, J. Jan

Department of Biomedical Engineering, FEEC, BUT, Brno, Czech Republic

asterios@feec.vutbr.cz

Abstract: 3D freehand ultrasound is an imaging technique, which is gradually finding clinical applications. A position sensor is attached to a conventional ultrasound probe, so that B-scans are acquired along with their relative locations. This allows the B-scans to be inserted into a 3D regular voxel array, which can then be visualized using arbitrary-plane slicing, and volume or surface rendering. A key requirement for correct reconstruction is the calibration: determining the position and orientation of the B-scans with respect to the position sensor's receiver. Following calibration, interpolation in the set of irregularly spaced B-scans is required to reconstruct a regular-voxel array. This text describes a freehand measurement of 2D ultrasonic data, an approach to the calibration problem and several numerical issues concerned with the calibration and reconstruction.

Introduction

Conventional 2D ultrasonic imaging uses a hand-held probe, which transmits ultrasound pulses into the body and receives the echoes. The magnitude and timing of the echoes are used to create a 2D grey-level image (B-scan) of a cross-section of the body in the scan plane. 3D ultrasonography extends this concept so that volumes of intensity data are created from pulse-echo information.

In 3D freehand ultrasonography a common ultrasonic probe is freely moved over the patient's body, so that the acquired B-scans have arbitrary relative locations and may overlap each other.

Electromagnetic or optical position-sensing devices, consisting of an electromagnetic transmitter and a receiver, or optical cameras and LED markers, respectively, are used to determine the position and orientation of the acquired B-scans. Before scanning, the receiver (or LED markers) is attached to the probe and the transmitter (or optical camera) is placed in a fixed position. The acquired B-scans and their relative positions are consequently used to fill a regular voxel array, which can then be visualized using arbitrary-plane slicing, multi-planar reformatting, volume rendering or surface rendering.

Both optical and electromagnetic position-sensing devices allow six degrees of freedom. The optical devices are supposed to be more accurate but at the same time more expensive and require full time optical contact between the camera and the LED markers. This is a quite difficult task when the 3D ultrasound is used as a tool for navigation during operation. The electromagnetic devices are less accurate than optical, since they are working on the base of transmitted and received electromagnetic waves, which can be influenced by surrounding electrically conducting devices and therefore lead to slightly inaccurate measurements. However, this error is not of such a degree that wouldn't allow them to be used for reconstruction of 3D ultrasound data, as seen from the large amount of publications on 3D ultrasound calibration where the correct use of electromagnetic devices is described.

We used the electromagnetic MiniBIRD position-sensing device (Ascension Technology Corporation). The transmitter transmits a pulsed DC magnetic field that is measured by the receiver. From the field characteristics, the MiniBIRD computes the position and orientation of the receiver. The sensor is capable of making up to 120 measurements/sec when it is located within 76 cm from the transmitter. The manufacturers claim a static resolution of 0.5 mm in change of position and 0.1˚ in change of orientation. The positional accuracy is 1.8 mm and the orientation accuracy 0.5˚. The pulsed DC technology employed by the MiniBIRD has minimal sensitivity to metal: five times less than AC technology.

Reconstruction

Figure 1 shows the four coordinate systems (c.s.) used for reconstruction. ***P*** is the c.s. of the B-scan plane, placed at the upper left corner of the B-scan. The y-axis is in the beam direction, the *x*-axis is in the lateral direction and the *z*-axis in the elevation direction, out of the B-scan plane. ***R*** is the c.s. of the moving receiver and ***T*** the c.s. of the fixed transmitter. The reconstruction volume, to be filled by the set of acquired B-scans, takes the form of a 3D matrix of voxels. ***C*** is its c.s. placed at its corner.

For every pixel in every B-scan we have to locate its corresponding voxel in the reconstruction volume. The vector ${}^{P}\mathbf{x}$ shows the location of each pixel in the B-scan, i.e. the distance of a pixel from ***P***. Each B-scan pixel's location, is transformed to ***R***, then to ***T*** and finally to ***C***. The overall transformation, which can be expressed as the multiplication of homogeneous transformation matrices, results in the vector ${}^{C}\mathbf{x}$ that represents the pixel's location in the coordinate system ***C***, i.e. the distance of each voxel from ***C***:

ISSN: 1727-1983

$$ {}^{C}\mathbf{x} = {}^{C}\mathbf{T}_{T}\ {}^{T}\mathbf{T}_{R}\ {}^{R}\mathbf{T}_{P}\ {}^{P}\mathbf{x} \quad (1) $$

$$ {}^{P}\mathbf{x} = \begin{pmatrix} s_x u & s_y v & 0 & 1 \end{pmatrix}^{T} \quad (2) $$

where ${}^{J}\mathbf{T}_{I}$ is the transformation from the c.s. ***I*** to the c.s. ***J***, u and v are the column and row indices of the B-scan pixels, and s_x and s_y are the scale factors of the pixels [mm/pixel]. The row and column indices of the cross-wire intersection point in the B-scan image can be detected either manually or automatically by a feature detection algorithm. Since the detectable point in the B-scan covers an area of several pixels, we can consider the middle pixel of the area as the one corresponding to the calibration point.

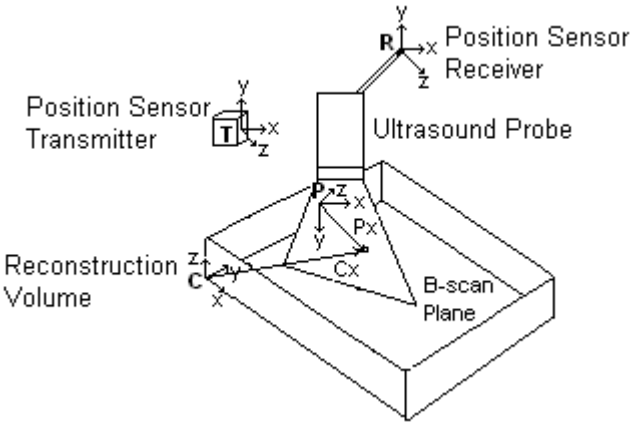

Figure 1: The four coordinate systems used during the reconstruction process

A transformation between two coordinate systems (c.s.) has six degrees of freedom: three rotations (α, β, γ) and three translations (x, y, z). The rotation between two c.s. is effected by first rotating e.g. through α around the x-axis, then through β around the y-axis, and finally through γ around the z-axis. Using this convention, the homogeneous matrix describing the transformation takes the following form:

$$ {}^{J}T_{I}(x,z,y,\alpha,\beta,\gamma) = \begin{pmatrix} \cos\alpha\cos\beta & \cos\alpha\sin\beta\sin\gamma - \sin\alpha\cos\gamma & \cos\alpha\sin\beta\cos\gamma + \sin\alpha\sin\gamma & x \\ \sin\alpha\cos\beta & \sin\alpha\sin\beta\sin\gamma + \cos\alpha\cos\gamma & \sin\alpha\sin\beta\cos\gamma - \cos\alpha\sin\gamma & y \\ -\sin\beta & \cos\beta\sin\gamma & \cos\beta\cos\gamma & z \\ 0 & 0 & 0 & 1 \end{pmatrix} \quad (3) $$

From the MiniBIRD readings we derive the transformation matrix ${}^{T}\mathbf{T}_{R}$, giving the position and orientation of ***R*** with respect to ***T***. The 6 parameters (rotations and translations) of ${}^{R}\mathbf{T}_{P}$, the 6 parameters of ${}^{C}\mathbf{T}_{T}$ and the 2 scale factors s_x and s_y, need to be determined by calibration.

Calibration

Calibration is performed by scanning a phantom of known geometric structure and dimensions. We can write equations similar to (1) using knowledge of the phantom geometry and the position sensor measurements. Solving the equations we determine the calibration parameters. Several calibration methods exist. Some rely on point targets such as small spheres [2] or intersection of thin wires [1]. Others detect plane targets as the bottom of a water bath [1], membranes [3, 6] or planes constructed from parallel wires [4, 5].

Cross-wire Calibration Phantom

It is the most commonly used phantom, because of the easiness to construct and scan it, and because it gives precise enough calibration results in comparison with other techniques [1].

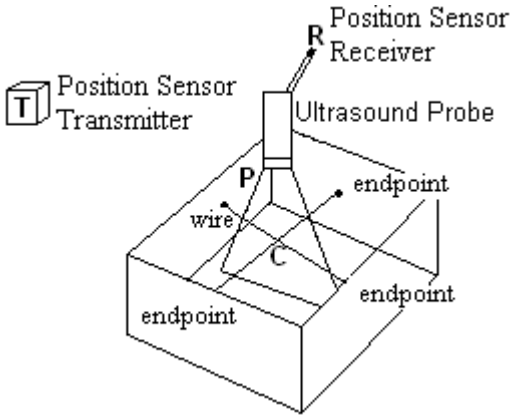

Figure 2: Cross-wire calibration phantom.

It consists of two very thin intersecting wires mounted on a wooden frame and inserted in water bath. We used nylon wires of 0.3 mm diameter. The transmitter was placed at some fixed location nearby (Fig. 2). The location where the wires cross has been repeatedly scanned from different directions. In each B-scan, a detectable cross-point appears. For calibration purposes, the origin of ***C*** is not regarded coincident with the corner of the reconstruction volume but with the wire intersection (Fig. 2). This makes the distance from the origin of ***C*** to the cross-wire point, i.e. the x, y and z components of the ${}^{C}\mathbf{x}$ vector, equal to zero. According to (1), the B-scan pixel at the centre of the cross should then satisfy the equation

$$ \begin{pmatrix} 0 & 0 & 0 & 1 \end{pmatrix}^{T} = {}^{C}\mathbf{T}_{T}\ {}^{T}\mathbf{T}_{R}\ {}^{R}\mathbf{T}_{P} \begin{pmatrix} s_x u & s_y v & 0 & 1 \end{pmatrix}^{T} \quad (4) $$

The first three rows of (4) give the three equations involving the measurements ${}^{T}\mathbf{T}_{R}$, u and v, and the unknowns ${}^{R}\mathbf{T}_{P}$, ${}^{C}\mathbf{T}_{T}$, s_x and s_y. If there are m B-scans, then the respective equations can be stacked together to produce a system of non-linear homogeneous equations of the size $3m = K$. We have measured 120 B-scans and therefore obtained a system of K=360 equations:

$$ \mathbf{f} = \{f_1, f_2, \ldots, f_K\} \quad (5) $$

or else

ISSN: 1727-1983

$$\mathbf{0} = \mathbf{f}(\boldsymbol{\theta}, \boldsymbol{\varphi}) \tag{6}$$

where $\boldsymbol{\theta}$ are the known quantities ${}^{T}\mathbf{T}_{R}$, u and v, while $\boldsymbol{\varphi}$ are the unknowns ${}^{R}\mathbf{T}_{P}$, ${}^{C}\mathbf{T}_{T}$, s_x and s_y. Therefore, $\boldsymbol{\varphi}$ is a 14-element vector, composed of the 6 parameters of ${}^{R}\mathbf{T}_{P}$, the 6 parameters of ${}^{C}\mathbf{T}_{T}$ and the two scale factors. However, the coordinate system $\boldsymbol{C}$ can be of any orientation and still satisfy (4). This means that the three orientation angles of ${}^{C}\mathbf{T}_{T}$ can be set to zero in (6) and only 11-elements of $\boldsymbol{\varphi}$ are to be found. Thus, a system of 360 equations, with 11 unknowns had to be solved.

Solving the system of non-linear equations

The algorithm used for the solution of this over-determined system is the Levenberg-Marquardt algorithm in frame of the Matlab's Optimization Toolbox (The Mathworks). The algorithm is iterative and tries to find the closest possible solution possibly avoiding local extrema. It needs an initial guess of the solution to the problem (a starting point). This guess could be any rough estimate of the true solution, but the closer it is to the true solution, the quicker the convergence. The initial estimate in a probe calibration can be found from a physical measurement of the translation with a ruler, and approximate knowledge about sensor orientation relative to the B-scan plane.

The Levenberg-Marquardt algorithm:

$$\begin{aligned} &\mathbf{0} = \mathbf{f}(\boldsymbol{\theta}, \boldsymbol{\varphi}) \approx \mathbf{f}(\boldsymbol{\theta}, \boldsymbol{\varphi}_{\mathbf{j}}) + \frac{\partial \mathbf{f}(\boldsymbol{\theta}, \boldsymbol{\varphi}_{\mathbf{j}})}{\partial \boldsymbol{\varphi}} \left(\boldsymbol{\varphi} - \boldsymbol{\varphi}_{\mathbf{j}}\right) \Rightarrow \\ &\Delta \mathbf{f} = \mathbf{J}\left(\boldsymbol{\varphi} - \boldsymbol{\varphi}_{\mathbf{j}}\right) = \mathbf{J}\,\Delta\boldsymbol{\varphi} \end{aligned} \tag{7}$$

where $\Delta\mathbf{f}$ is the error vector $-\mathbf{f}(\boldsymbol{\theta}, \boldsymbol{\varphi}_{\mathbf{j}})$ and $\mathbf{J}$ is the gradient matrix $\partial\mathbf{f}(\boldsymbol{\theta}, \boldsymbol{\varphi}_{\mathbf{j}})/\partial\boldsymbol{\varphi}$, also known as the Jacobian. The Levenberg-Marquardt algorithm produces the updated parameter vector values $\boldsymbol{\varphi}_{\mathbf{j+1}}$:

$$\boldsymbol{\varphi}_{\mathbf{j+1}} = \boldsymbol{\varphi}_{\mathbf{j}} + \left(\mathbf{J}^{T}\,\mathbf{J} + \varepsilon\ \mathbf{I}\right)^{-1} \mathbf{J}^{T}\,\Delta\boldsymbol{\varphi} \tag{8}$$

where ε is a damping term chosen at each step to stabilize the convergence. This method becomes the standard iterative least squares algorithm for $\varepsilon = 0$. At each step, $\Delta\mathbf{f}$ and $\mathbf{J}$ are evaluated at the current estimate $\boldsymbol{\varphi}_{\mathbf{j}}$. This process is iterated until the corrections $\Delta\boldsymbol{\varphi}$ are sufficiently small.

In case that the input data (number of B-scans and corresponding probe positions and angles) are numerous and differ from each other (covering all possible probe angles and positions), the algorithms converge quickly to a precise solution

A comment on mirror solutions

Several distinct angles and scales produce the same calibration. We call these "mirror solutions". In order to compare solutions, we have to adopt a canonical form for the angles and scales. This requires that

- s_x and s_y are positive,
- α and γ are in the range $\pm\pi$,
- β is in the range $\pm\pi/2$.

Procedure [1] for enforcing these constraints:

- Limit all the angles to the range $\pm\pi$ by adding or subtracting $k2\pi$.
- If β is outside of $\pm\pi/2$, add or subtract π to correct it, and add π to both α and γ.
- If $s_y < 0$, change γ to $\gamma+\pi$ and s_y to $-s_y$.
- If $s_x < 0$, change α to $\alpha+\pi$, β to $-\beta$, and s_x to $-s_x$.
- Check that α and γ are still within $\pm\pi$. If not, repeat the step 1.

Automatic Segmentation of the calibration features

In the initial phase of the work, the detectable cross-points on each B-scan were manually segmented, using a graphical user interface developed in MatLab environment, i.e. by selecting the middle pixel of the cross-point and computing its (u, v) coordinates. The segmentation had been done independently 5 times for each B-scan and the results had been averaged.

In several texts about 3D freehand ultrasound calibration with phantoms consisting of point targets, it is stated that the segmentation of the point targets has to be done manually because the high speckle noise on the calibration B-scans would make an automatic detection algorithm to fail. This makes the calibration process too time and effort consuming. Followingly we are presenting an approach fo automatic segmentation of the point calibration features.

During the calibration measurement the System's FiVe function "tissue amplification" had been used. The overall tissue amplification as seen on the resulted B-scan image can be adjusted using the "2D Gain" knob. Setting this value to minimum yields low signal amplification and as a further result the speckle noise, reflections from bubbles, and dust decrease and in some cases almost disappear. The reflection from the cross-point decreases too, but still remains the strongest reflection among all others. Also care has been taken not to have reflections from the walls of the phantom on the B-scan images. Therefore, images have been obtained where the reflection from the cross-point is quite bright and the noisy reflections quite dark.

Now having images where the reflection of the cross-point is the only strong reflection on the image, we could perform a thresholding that would leave just a few bright pixels that correspond to the cross-point. From these pixels the intensity centroid was computed, which corresponds to the cross-point center.

Calibration Precision Evaluation

Two approaches have been used for the evaluation of the calibration precision: the residual value and the mean point reconstuction. A detailed dscription follows.

Solving the system of calibration equations (functions) $\mathbf{f} = \{f_1, f_2, \ldots, f_K\}$ with an iterative algorithm

ISSN: 1727-1983

such as the Levenberg-Marquardt we obtain an estimation of the calibration parameters. Replacing those parameters back to the system of equations we get the value of each function itself. The lower the value of a concrete function the best the fit of the estimated parameters for this concrete equation. In an ideal case this value should be 0 and the fit could then be regarded as absolute. In a non-linear system formed of tenths of equations containing several unknown parameters such as the case of the calibration system an absolute fit is impossible. That is also the reason that the solution of the system is referred to as an estimation and not as an absolute solution. Residual is termed the sum of the squared function values (9) and has been used in this work as a metric of precision

$$R = \sum_{i=1}^{K} f_i^2 \tag{9}$$

The smaller the residual value the more precise the estimated parameters and the whole calibration process.

Another method involves imaging a cross-wire from multiple viewing angles. The generated "points" are then extracted from each image and mapped in the coordinate system ***C*** of the reconstruction volume, ultimately forming a cloud of points. The parameters describing the tightness of this cloud have been used to estimate the mean point reconstruction precision.

Calibration Accuracy Evaluation

Similarly to the experiment evaluating the mean point reconstruction precision with a cross-wire, it is also possible to estimate the mean point reconstruction accuracy if the position of the cross-wire is known in the transmitter's coordinate system (c.s.) ***T***. The average point position of the cloud of points is computed and then compared to the known "gold standard" position value. The smaller the distance, the best the accuracy.

The position of the cross-wire point with respect to the ***T*** can be computed by the use of a calibrated pointer. The calibrated pointer consists of a wooden stick, at the one edge of which, the MiniBIRD's receiver is mounted and on the other edge a thin pin. The transmitter is fixed nearby. The pin is placed in a fixed point q, and a rotation over all possible angles is performed. The MiniBIRD is all the time sensing the position and orientation of the origin of the receiver's c.s. ***R*** with respect to the origin of the transmitter's c.s. ***T***. For the fixed point q holds:

$$\bar{0} = {}^{q}\mathbf{T}_{T} \cdot {}^{T}\mathbf{T}_{R} \cdot {}^{R}\mathbf{x}_{q} \Rightarrow$$

$$\begin{pmatrix} 0 \\ 0 \\ 0 \\ 1 \end{pmatrix} = \begin{pmatrix} {}^{q}x_{T} \\ {}^{q}y_{T} \\ {}^{q}z_{T} \\ 1 \end{pmatrix} \begin{pmatrix} \cos\alpha\cos\beta & \cos\alpha\sin\beta\sin\gamma - \sin\alpha\cos\gamma & \cos\alpha\sin\beta\cos\gamma + \sin\alpha\sin\gamma & {}^{T}x_{R} \\ \sin\alpha\cos\beta & \sin\alpha\sin\beta\sin\gamma + \cos\alpha\cos\gamma & \sin\alpha\sin\beta\cos\gamma - \cos\alpha\sin\gamma & {}^{T}y_{R} \\ -\sin\beta & \cos\beta\sin\gamma & \cos\beta\cos\gamma & {}^{T}z_{R} \\ 0 & 0 & 0 & 1 \end{pmatrix} \begin{pmatrix} {}^{R}x_{q} \\ {}^{R}y_{q} \\ {}^{R}z_{q} \\ 1 \end{pmatrix} \tag{10}$$

From left to right: ${}^{R}\mathbf{x}_{q}$ is a homogeneous 4x1 vector containing the unknown distances ${}^{R}x_{q}$, ${}^{R}y_{q}$, ${}^{R}z_{q}$, from the fixed point q to the origin of the c.s. R. ${}^{T}\mathbf{T}_{R}$ is a homogeneous 4x4 transformation matrix from the origin of ***R*** to the origin of ***T***. Contains the known position and orientation parameters of ***R*** with respect to the ***T***. ${}^{q}\mathbf{T}_{T}$ is a homogeneous 4x1 vector containing the unknown distances ${}^{q}x_{T}$, ${}^{q}y_{T}$, ${}^{q}z_{T}$, from the origin of ***T*** to the point q. The product of the vectors and matrices result in a transformation from the fixed point q back to q. Thus it should equal to a homogeneous 4x1 zero-vector.

The MiniBIRD system measured m different locations (in the order of hundreds) of the receiver and therefore m different ${}^{T}\mathbf{T}_{R}$ matrices. The first 3 rows of the zero-vector in (10) correspond to 3 equations Thus a system of $3m$ equations with 6 unknowns has been created: distance ${}^{q}x_{T}$, ${}^{q}y_{T}$, ${}^{q}z_{T}$ of the origin of ***T*** from the point q and distance ${}^{R}x_{q}$, ${}^{R}y_{q}$, ${}^{R}z_{q}$ of point q from the origin of the ***R***. This system can be solved using the Levenberg-Marquardt iterative algorithm. Thus the calibrated pointer can be used to compute the distance between any point and the transmitter or the receiver.

This method has been used to measure the position of the cross-wire with respect to the origin of ***T***. The calibrated pointer was placed at the four endpoints of the cross-wire phantom, which are mounted on the wooden frame (Fig. 1), and a rotation of the pointer was performed. Now knowing the position of the endpoints with respect to ***T*** we can also compute the position of the cross-wire point (line-line intersection in 3D problem) with respect to ***T*** and then compare it with the average position of the mapped calibration points in ***T***.

Automatic Detection and Discarding of "Bad" B-scans

To our surprise, the computed residual value, after solving the system of equations for the estimation of the calibration parameters, was too high (equal to *902.391*). Our belief was that using a great number of calibration B-scans which cover all possible positions and orientations of the probe with respect to the stable electromagnetic transmitter, would result to a precise calibration and therefore to a small residual value.

Having a more careful look at each B-scan separately, it was found out that some of the detectable calibration B-scan features probably did not correspond to the real wire intersection. Therefore these 'bad' B-scans had to be discarded. For example, deleting just two "bad" B-scans lead in a decrease of the residual value to *615.458*. The manual, visual examination of each image is time consuming because of the great amount of images to be examined. Therefore we created an automatic "bad" B-scan discarding method.

After solving the system of non-linear equations, the 11 unknown parameters were replaced with the estimated ones, and the computed function values were examined. To the sequence of 120 B-scans correspond 360 equations and therefore 360 function values. Every three successive function values correspond to one B-scan (11). This way I divide the set of 360 function values to 120 triplets as shown below (11).

ISSN: 1727-1983

$$\mathbf{f}=\{f_1, f_2, f_3, f_4, f_5, f_6, \ldots, f_{355}, f_{356}, f_{357}, f_{358}, f_{359}, f_{360}\} \quad (11)$$

1st B-scan 2nd 119th 120th B-scan

Then we found the triplets that corresponded to the B-scans that we previously classified manually as "bad" ones and we saw that they contained very high absolute values, in some cases greater than 12. Notice that the function values should be ideally 0 or at least less than 1. It has thus been found a criterion decisive for classifying a B-scan as a good or bad. Therefore, I could now automatically discard all those B-scans for which the corresponding triplets contained absolute values greater than the threshold value 1, since they obviously are "bad" B-scans. Also notice that with the visual examination of the images I was not able to detect all "bad" images. Therefore the automatic method based on the function values does not only fasten the process of bad B-scan discarding, but also makes it more accurate

Numerical Results

Solution of the initial system of 120 B-scans (360 equations)

Table 1: Numerical results from the solution of the system of all 120 cross-wire calibration B-scans

# of B-scans	120
Starting point x_0 (selected randomly)	$\alpha = \pi/25$ rad, $\beta = 5/3*\pi$ rad, $\gamma = \pi/3$ rad, $s_x = 0.1$ mm/pixel, $s_y = 0.15$ mm/pixel, ${}^{R}x_P = 5$ mm, ${}^{R}y_P = 45$ mm, ${}^{R}z_P = 89$ mm, ${}^{C}x_T = 60$ mm, ${}^{C}y_T = 15$ mm, ${}^{C}z_T = 300$ mm
Residual	902.391
Resulting estimated parameters after correction of mirror solutions	$\alpha = 1.5389$ rad, $\beta = 0.0402$ rad, $\gamma = 0.5327$ rad, $s_x = 0.2835$ mm/pixel, $s_y = 0.2955$ mm/pixel, ${}^{R}x_P = -34.9345$ mm, ${}^{R}y_P = -73.1145$ mm, ${}^{R}z_P = 205.1628$ mm, ${}^{C}x_T = -37.9614$, ${}^{C}y_T = 131.4386$ mm, ${}^{C}z_T = 350.7175$ mm
Triplets containing function absolute values smaller than 1: 55	
Triplets containing function absolute values greater than 1: 65	

From the table 1, it becomes obvious that the calibration precision is too low since the residual value is too high and a great number of functions (65 out of 120) have an absolute value greater than the threshold value 1. In some cases this value was greater than 12.

The bad precision becomes more obvious by mapping the calibration points from each B-scan (c.s. ***P***) to the c.s. of the reconstruction volume ***C***. The computed parameters from the system of 120 B-scans (Table 1) have been used in order to do so. The mapped points in ***C*** look like a cloud of points (Fig. 3).

The statistic values describing the scatter of the cloud are presented in table 2; the minimum and maximum coordinates (or position) of the cross-points in ***C***, the range of spread as a sum of the absolute maximum and minimum value, the mean position, the standard deviation and the variance in each of the three dimensions *x*, *y*, and *z*.

From the table 2 next, it is obvious that the precision is too low. The extend of the area of mapped points to the coordinate system of the reconstruction volume ***C*** (range) is too big. Especially in *x* and *y*-axis where it exceeds 20 and 14 mm, respectively. This would obviously yield an incorrect reconstruction. This unsatisfactory result indicated the necessity to detect and delete the "bad" B-scans.

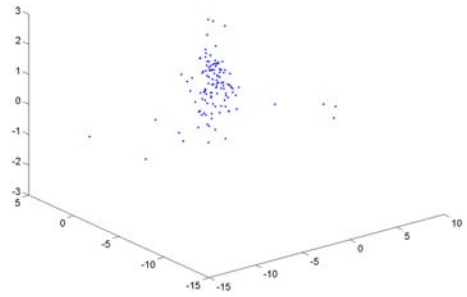

Figure 3: Mapping of the calibration point from each B-scan to the c.s. ***C*** of the reconstruction volume.

Table 2: Mean Point Reconstruction Precision Evaluation for the system of 120 calibration B-scans

	X	Y	Z
Min. position [mm]	-12.2711	-11.3199	-2.0746
Max. position [mm]	8.2633	2.8506	2.2534
Range[mm]	**20.5344**	**14.1704**	**4.3281**
Mean position [mm]	5.0190e-004	-9.1889e-004	0.0079
Standard Deviation	2.1009	1.5988	0.7833
Variance	4.4136	2.5561	0.6135

We continued evaluating the calibration accuracy. We had to map the B-scan cross-points to the coordinate system ***T*** of the fixed transmitter and compute the average position of the mapped points. The range in T-space, the standard deviation and the variance of the cloud remain naturally the same as with the table 2 where they were mapped to C-space. The parameter of interest here is the mean mapped position (Table 3).

Then, using the calibrated pointer we measured the positions of the 4 endpoints of the wires with respect to the origin of ***T***. This has been done 4 times and average endpoint positions have been computed. From the endpoint positions I further computed the wire intersection position with respect to ***T***. Finally I compared the mapped position with the computed position. The difference between those two positions expresses the calibration accuracy.

Table 3: Mean Point Reconstruction Accuracy Evaluation for the system of all 120 calibration B-scans

Wire intersection pos. in ***T***	*X*	*Y*	*Z*
Mean mapped position [mm]	-37.9619	131. 4395	350. 7096
Computed position [mm]	-39.067	131.052	347.4565
Absolute Difference (Accuracy Error) [mm]	**1.1051**	**0.3875**	**3.2531**

From the table above it is obvious that the accuracy of the cross-wire calibration is rather good. In specific, the accuracy of reconstructing a point in world space has an error of 1.1051 mm in *x*, 0.3875 mm in *y*, and

ISSN: 1727-1983

3.2531 mm in *z*. Discarding the "bad" B-scans will furthere increase the accuracy.

Solution of the Reduced System of 66 B-scans (198 equations)

The first attempt to increase the calibration precision and accuracy was by deleting the two bad B-scans that corresponded to triplets containing absolute function values greater than 11 and 12. This yields a system of 118 B-scans with residual decreased to *615.458*. Deleting one more B-scan corresponding to a triplet having the value greater than 8 decreases the residual to *522.678*. I continued this way deleting the triplets that contained high absolute values and checking the residual. I stopped when all remained triplets contained absolute values less than 1. This was for the system of 66 images (3x66=198 equations). The number of equations was still adequate enough to create an over-determined system and the residual decreased substantially to **45.5311**, which is small enough compared to the great number of equations (198). The final numerical results are presented in tables 4, 5, 6.

Table 4: Numerical results from the solution of the reduced system of 66 cross-wire calibration B-scans.

# of B-scans	66
Starting point x_0	the same as in table 1
Residual	45.5311
Resulting estimated parameters after correction of mirror solutions	α = 1.5495 rad, β = 0.0362 rad, γ = 0.5193 rad, s_x = 0.292 mm/pixel, s_y = 0.3008 mm/pixel, ${}^{R}x_P$ = -32.185 mm, ${}^{R}y_P$ = -73.8979 mm, ${}^{R}z_P$ = 205.2409 mm, ${}^{C}x_T$ = -38.1767 mm, ${}^{C}y_T$ = 131.443 mm, ${}^{C}z_T$ = 350.6575 mm
Triplets containing function absolute values smaller than 1: 66	

Table 5: Mean Point Reconstruction Precision Evaluation for the reduced system of 66 B-scans

	X	Y	Z
Minimum position [mm]	-0.9974	-0.7405	-0.9618
Maximum position [mm]	0.9776	0.923	0.9495
Range [mm]	**1.975**	**1.6635**	**1.9113**
Mean position[mm]	-0.0018	-0.0047	-0.0152
Standard Deviation	0.4847	0.4219	0.5365
Variance	0.2349	0.178	0.2878

Therefore, the range of mapping a cross-point to the ***C*** has been know decreased to 1.975 mm in x, 1.6635 mm in y and 1.9113 mm in z yielding a very good precision.

In the brackets of table 6 are the old values from the table 3 (system of 120 B-scans) for comparison. The accuracy in *x* and *z* have increased and in *y* has a little bit decreased. The accuracy in *x* and *y* is very high but in *z* is smaller. This can be explained by the fact that the *z* direction was not covered so well during the measurement as the *x* and *y* directions. The *z* direction was the one perpendicular to the floor of the water tank inside which the phantom was mounted. The motion of the probe in this direction was limited because the phantom had been placed only a few centimetres below the surface of water. In a future measurement this mistake will be avoided by placing the phantom deeper inside the water tank.

Table 6: Mean Point Reconstruction Accuracy Evaluation for the reduced system of 66 B-scans.

Wire intersection pos. in ***T***	*X*	*Y*	*Z*
Mean mapped position [mm]	-38.1749	131. 4395	350.6727
Computed position [mm]	-39.067	131.052	347.4565
Absolute Difference (Accuracy Error) [mm]	**0.8921** (1.1051)	**0.3957** (0.3875)	**3.2162** (3.2531)

Conclusions

The cross-wire calibration technique has been implemented and tested yielding very good results from the point of view of calibration accuracy and precission. At the same time the cross-wire phantom is eacy to construct and scan. The time and effort consuming part of manual calibration-feature segmentation has been avoided by the implementation of a simple but effective automatic method. Furthermore, a method for automatic detection and discarding of the bad B-scans containing features not corresponding to the center of the cross-wire, has been implemented, improving the calibration precission and accuracy.

References

[1] PRAGER R., ROHLING, R., GEE, A., BERMAN, L. (1998): 'Rapid calibration for 3D freehand ultrasound', *Ultrasoun in Medicine and Biology*, **24**, pp. 855 - 869

[2] AMIN D., KANADE T., JARAMAZ B., DiGIOIA A., NIKOU K., LaBARCA R., MOODY, J. (2001): 'Calibration method for determining the physical location of the ultrasound image plane'. Lecture Notes in Computer Science, **2208**, pp. 940-947.

[3] LANGR T., LINDSETH F., KASPERSEN J.(2000): 'Novel probe calibration methods for 3D freehand ultrasound', Submitted to *Computer Aided Surgery*.

[4] LEOTTA, D. (2004): 'An efficient calibration method for freehand 3D ultrasound imaging system', *Ultrasound in Medicine and Biology*, **30**, pp. 999-1008.

[5] BOUCHET L., MEEKS S., GOODCHILD G. (2001): 'Calibration of 3D ultrasound images for image-guided radiation therapy', *Physics in Medicine and Biology*, **46**, pp. 559–577.

[6] SATO, Y., NAKAMOTO, M., TAMAKI. K. (1998): 'Image guidance of breast cancer surgery using 3D US images and augmented reality visualization', *IEEE Transactions in Medical Imaging* **17**, pp. 681–693.

ISSN: 1727-1983